Quantum Computing for Analyzing Array Antenna Power Patterns

L. Tosi, P. Rocca, N. Anselmi, and A. Massa

2024/07/26

Contents

1 Introduction

The following report is aimed at assessing how the Quantum Fourier Transform (QFFT) algorithm can be exploited for the analysis of Phased Arrays. The assessment will be carried out in three main phases:

1. **Validation** of the method: prove that if a qubit register is initialized with a set of excitations, by applying the QFFT operation, it is possible to retrieve the Power Pattern generated by a Phased Array fed with the same excitations.
2. **Assessment** of the framework: analyze the effect of the variation of number of shots (T) used for the computation of the QFFT, also in relation to different excitations scenarios.
3. **Real Quantum Computer Assessment**: test the procedure on real quantum computers with dedicated test cases.
4. **Computational cost analysis**: analyze the conditions under which calculating the Power Pattern of an array using the QFFT is more convenient than using classical procedures and algorithms in terms of computational complexity.

2 Mathematical Formulation

2.1 QFFT Generated Power Pattern

Classic Power Pattern

Let us consider a linear Phased Array composed of N equispaced elements along the z axis, and having complex excitations $\underline{w} = \{w_n : n = 0, \ldots, N-1\}$. In order to properly initialize the excitations vector, it is necessary to take into account the fact that the input of the QFFT must have the same length of the output, as the number of qubits involved is fixed during the transformation the process. It is therefore mandatory to zero pad the excitations vector with $M - N$ values, leaving the final length of $\underline{w}$ to M. The radiation pattern generated by the array is given by the array factor A:

$$A(u) = \sum_{n=0}^{M-1} w_n e^{jkndu} \tag{1}$$

where $u = cos(\theta)$ is the cosine angular direction, $k = 2\pi/\lambda$ is the wave number given the wavelength λ and d is the inter-element spacing. The expression of A can be written as function of a set of M discrete angular samples $A(u_m)$, so that the relationship between the set of excitations $\underline{w}$ and $A(u_m)$ is a Discrete Fourier Transform (DFT). More specifically:

$$A(u_m) = A_m = \sum_{n=0}^{M-1} w_n e^{-2\pi j \frac{nm}{N}} \tag{2}$$

for each $m = 1, \ldots, M$. The function $A(u)$ can be recovered from the A_m samples by means of a weighted summation of sinc functions, $S(x) = sin(Nx)/Nsin(x)$ as:

$$A(u) = \sum_{m=0}^{N-1} A_m S(\pi du + \frac{m\pi}{N}) \tag{3}$$

Given the array factor A, the corresponding power pattern generated by the array is

$$P(u) = |A(u)|^2 \tag{4}$$

The same relationship holds true for the discretized version, and considering $P_m = P(u_m)$ to be the $m-$th angular sample it can be stated that:

$$P_m = |A_m|^2 \tag{5}$$

Quantum Power Pattern

To generate a phased array power patter to quantum computing the process only consists in applying the Quantum Fourier Transform (QFFT) to the set of excitations; the procedure is described in the following.

The first step is to initialize a qubit vector $|w\rangle$ to define the input state vector of $L = \lceil log_2(M) \rceil$ qubits such that:

$$|w_n\rangle = \sum_{n=0}^{M-1} \hat{w_n} |b_n\rangle \tag{6}$$

where $\hat{w_n} = w_n / \|\underline{w}\|$, $n = 1, \ldots, N$, being $\|\cdot\|$ the norm operator and $|b_n\rangle = |q_L^{(n)}, \ldots, q_1^{(n)}\rangle$ the multi-qubit state originated by the concatenation of the L qubits. Similarly to the classical version, when the QFFT algorithm is applied to the $|w\rangle$ vector, the result will be a set of M complex values associated to the output state vector related to the m-th angular samples of the array factor, namely

$$\sum_{n=0}^{M-1} \hat{w_n}|b_n\rangle \rightarrow \sum_{m=0}^{M-1} A_m|b_m\rangle \tag{7}$$

However, the outputs observable from the QFFT will be the probability p_m, $m = 1, \ldots, M$ of measuring each state $|b_m\rangle$. Indeed the following relationship holds:

$$\hat{p_m} = |A_m|^2 \tag{8}$$

where $\hat{p_m} = p_m / p_{max}$, being $p_{max} = max\{p_m\}$, $m = 1, \ldots, M$ the maximum probability among the output state vector. Given the normalized probability, applying a circular shift th the indexes of $M/2$ positions and inverting their order, the power pattern is obtained as:

$$P_m = \hat{p_m}$$

2.2 Power Pattern Mismatch Metric Definition

To quantify the precision of the QFFT, using a number of shots T, in replicating a power pattern $P_{ref}(u)$ derived from a set of excitations $\underline{w} = \{w_n, n = 1, ..., N\}$ with $w_n = \alpha_n e^{j\beta_n}$ the following metric is adopted

$$\Gamma^{(T)} = \frac{\sum_{u=-1}^{u=1} \left| |E_{ref}(u)|^2 - P_{QFFT}^{(T)}(u) \right|}{\sum_{u=-1}^{u=1} |E_{ref}(u)|^2} \tag{9}$$

Region Dependent Error Metric

Since the largest part of the error seems due to errors in the side lobes (SL) region, error is computed with a region dependent approach, dividing in SL and main lobe (ML) regions.

Error in the ML region $\Gamma_M^{(T)}$ is defined as:

$$\Gamma_M^{(T)} = \frac{\sum_{u=\nu}^{u=\chi} \left| |E_{ref}(u)|^2 - P_{QFFT}^{(T)}(u) \right|}{\sum_{u=-1}^{u=1} |E_{ref}(u)|^2} \tag{10}$$

where χ is the u coordinate of the first null to the right of the main lobe and ν is the first null to the left of the main lobe.

Error in the SL region $\Gamma_S^{(T)}$ is defined as:

$$\Gamma_S^{(T)} = \frac{\sum_{u=\chi}^{u=1} \left| |E_{ref}(u)|^2 - P_{QFFT}^{(T)}(u) \right| + \sum_{u=-1}^{u=\nu} \left| |E_{ref}(u)|^2 - P_{QFFT}^{(T)}(u) \right|}{\sum_{u=-1}^{u=1} |E_{ref}(u)|^2} \tag{11}$$

The constraint on both errors is that:

$$\Gamma_s^{(T)} + \Gamma_M^{(T)} = \Gamma^{(T)} \tag{12}$$

Statistical Measurements on Errors

Since each pattern generated by the QFFT is only a realization of a random process, the same error is calculated over R repetitions, in order to obtain statistical measurements, in particular the average error, Γ_{avg} and the variance Γ_{var}, computed as:

$$\Gamma_{avg}^{(T)} = \frac{1}{R} \sum_{r=1}^{R} \Gamma_r^{(T)} \tag{13}$$

$$\Gamma_{var}^{(T)} = \frac{1}{N-1} \sum_{r=1}^{R} \left(\Gamma_r^{(T)} - \Gamma_{avg}^{(T)} \right)^2 \tag{14}$$

2.3 QFFT Resolution Limits

The output of the Qiskit software computing the QFFT operation can be seen as a vector, whose indexes are the number of a state m, to which is associated a value μ_m, representing the number of times the m^{th} state has been measured at the measurement gate. The probability of each state is therefore computed as $p_m = \mu_m / T$.

To represent the Power Pattern related to a set of excitations, to the m^{th} angular sample u_m is associated a value $P(u_m)$, which is calculated starting from μ_m as:

$$P(u_m) = \frac{p_m}{p_{max}} = \frac{\mu_m / T}{\mu_{max} / T} = \frac{\mu_m}{\mu_{max}} \tag{15}$$

Besides the case in which a state m is not measured, (and therefore $\mu_m = 0$ and $p_m = 0$), the minimum representable power value is $\delta = 1/\mu_{max}$, which can be represented as

$$\delta = -10 log_{10} \mu_{max} [\text{dB}] \tag{16}$$

From the previous observation it is clear that if $\mu_{max}$is derived from a larger value of T, it will be able to represent even lower probability states.

It must be noticed that the minimum representable value δ can *be* computed only after the measurement procedure has ended.

This is due to the fact that each new measurement of the output state could lead to a new sample in the maximum number of counts per state.

3 Validation

The goal of this section is to prove the theoretical assumption that applying the QFFT algorithm to a qubit vector initialized with excitations, the output is a statevector which coefficients follow the power pattern of an equivalent array. In the following, a comparison of the power pattern obtained via classical computing method (squaring the module of DFT otput) is compared with the bare QFFT algorithm application to the excitations qubit vector. Since this test is done to prove the validity of the method an arbitrary high value of T, $(T \gg M)$ has been chosen, so to reduce the statistical variance in the QFFT output.

Parameters:

Array Parameters:

- Number of elements (N): 16
- Elements spacing (d): $\lambda/2$
- Excitation Distribution: Dolph-Chebychev (Real Excitations)
- SLL: -15 [dB]

DFT/QFFT Parameters:

- Number of DFT/QFFT points (M): 1024
- Number of QFFT shots (T): 10^6

Numerical Results:

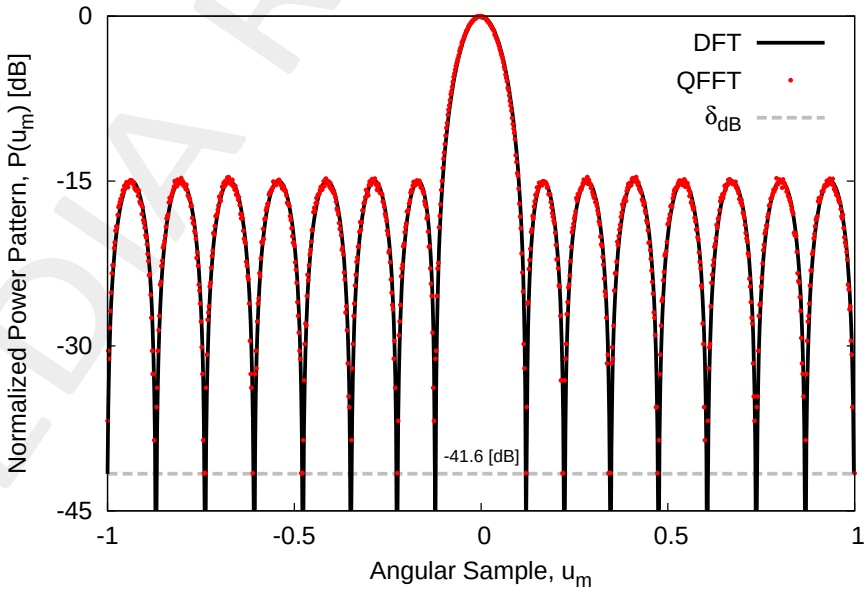

Figure 1: *Validation* ($N = 16$, $M = 1024$, $T = 1.024 \times 10^6$, $SLL = -15$ [dB]) - Comparison between Power Pattern Generated by DFT and QFFT algorithms, and QFFT resolution limit δ according to Eq.16 (dashed line)

Observations

For the plot of Fig. 1 the number of shots μ_{max}, related to the maximum probability state, is 1.4518×10^4, therefore, following Eq. 16, the resolution in decibel is -41.619 [dB], in correspondence with the set of minimum probability points within the plot.

4 Assessment

In this section, the validity of the method is assessed in relation to different power patterns, as the method should be able to replicate the pattern generated by any set of excitations. Since the main challenge for the QFFT based approach is reaching a good resolution, this section has the goal of showing the dependency between the number of shots used in the probability estimation and the SLL of the target power pattern. A Dolph-Chebychev distribution is selected for all the tests in order to better relate the resolution of the QFFT to the minimum representable power level.

4.1 Single SLL analysis

Parameters

Array Parameters:

- Number of elements (N): 16
- Elements spacing (d): $\lambda/2$
- Excitation Distribution: Dolph-Chebychev (Real Excitations)
- SLL cases: -15, -20, -25 [dB]

DFT/QFFT Parameters:

- Number of DFT points (M):1024
- Shots interval [$T_{min} : T_{step} : T_{max}$]: $T_{min} = 2.048 \times 10^3 (M \times 2)$, $T_{max} = 1.024 \times 10^5 (M \times 100)$, $T_{step} = 1.024 \times 10^3$ (M)
- QFFT repetitions (R): 20

To assess how the QFFT output approximates the classical power pattern, a single realization of the QFFT output is reported for each SLL value.

4.1.1 SLL=-15 [dB]

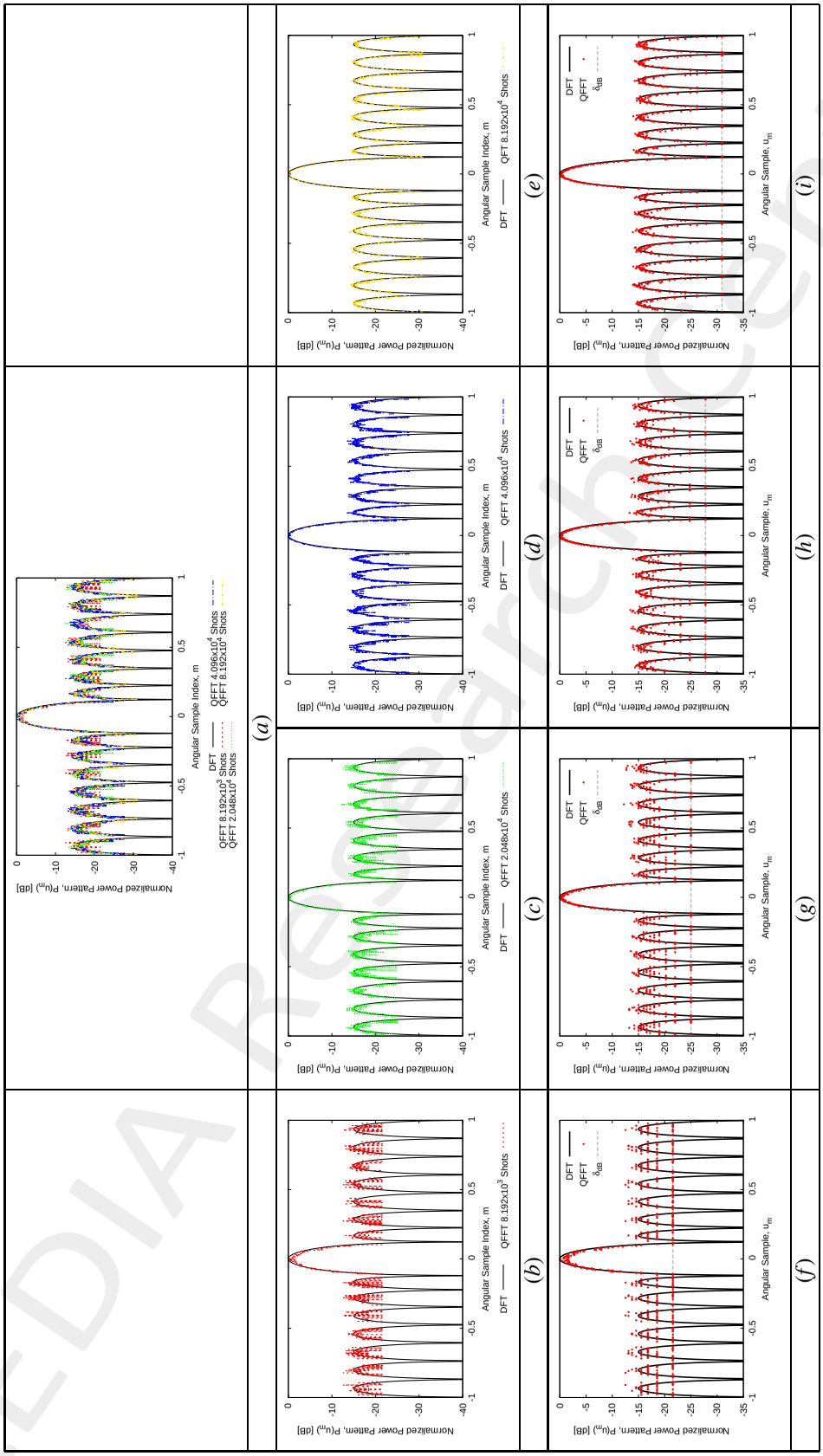

Figure 2: *Assessment - SLL variation analysis* ($N = 16$, $M = 1024$, $T \in \left[8.192 \times 10^3 : 8.192 \times 10^4\right]$, $SLL = -15$ [dB]) - Example of QFFT Power Patterns compared with FFT generated Reference Patterns when (*b*)(*f*) $T = 8.192 \times 10^3$, (*c*)(*g*) $T = 2.048 \times 10^4$, (*d*)(*h*) $T = 4.096 \times 10^4$, (*e*)(*i*) $T = 8.192 \times 10^4$

4.1.2 SLL=-20 [dB]

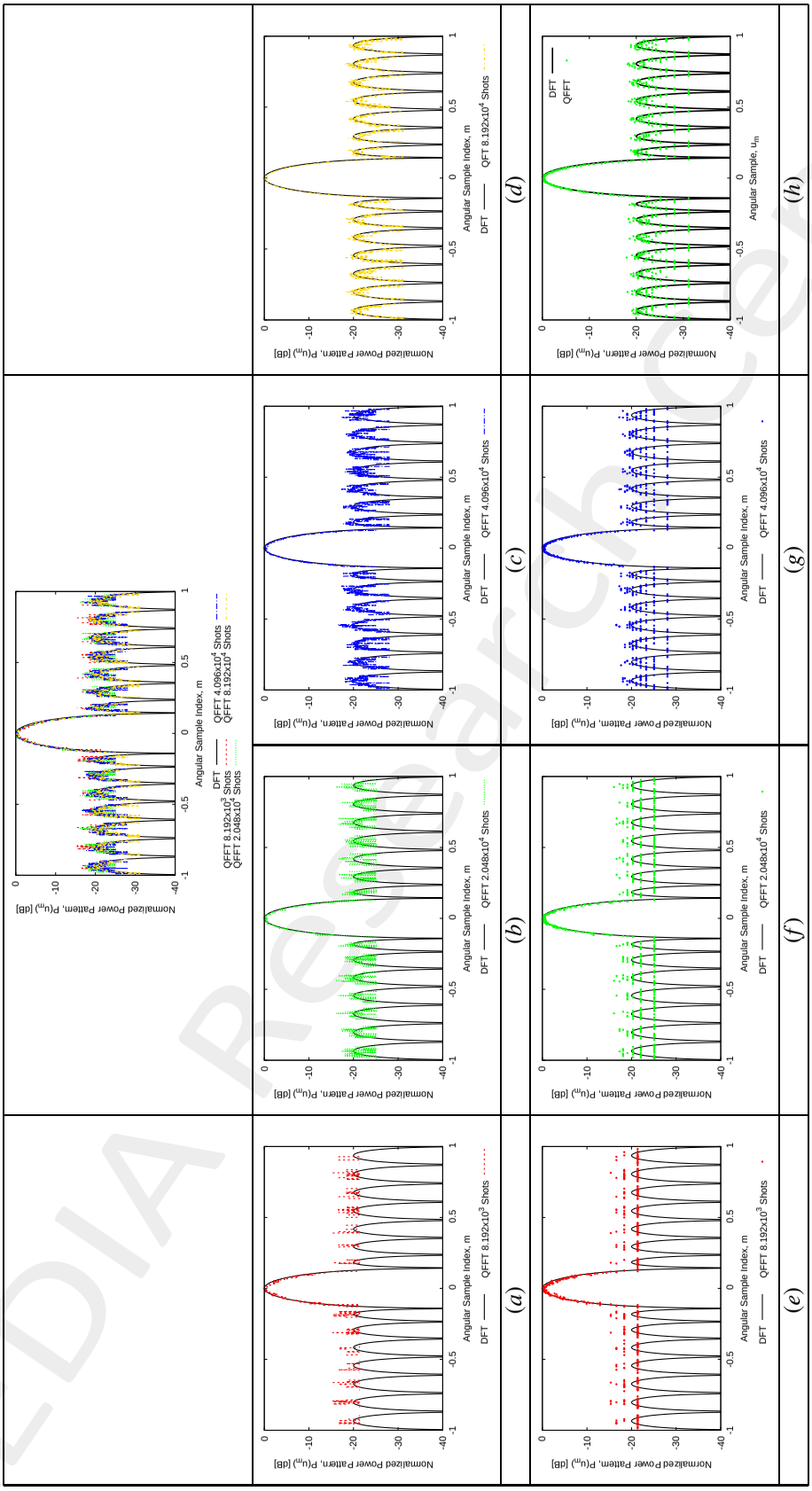

Figure 3: *Assessment - SLL variation analysis* ($N = 16$, $M = 1024$, $T \in \left[8.192 \times 10^3 : 8.192 \times 10^4\right]$, $SLL = -20$ [dB]) - Example of QFFT Power Patterns compared with FFT generated Reference Patterns when (*b*)(*f*) $T = 8.192 \times 10^3$, (*c*)(*g*) $T = 2.048 \times 10^4$, (*d*)(*h*) $T = 4.096 \times 10^4$, (*e*)(*i*) $T = 8.192 \times 10^4$

4.1.3 SLL=-25 [dB]

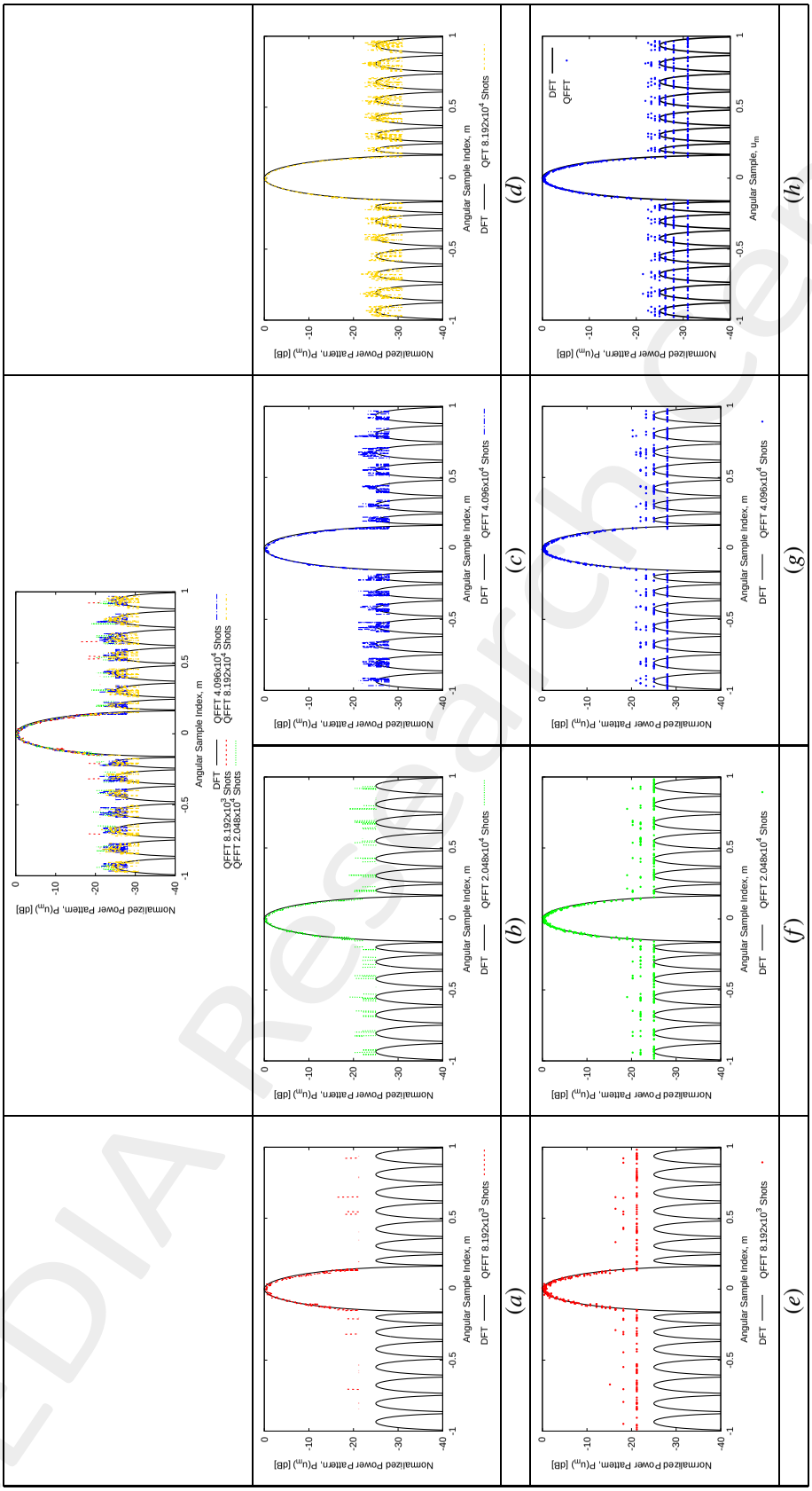

Figure 4: *Assessment - SLL variation analysis* ($N = 16$, $M = 1024$, $T \in \left[8.192 \times 10^3 : 8.192 \times 10^4\right]$, $SLL = -25$ [dB]) - Example QFFT Power Patterns comparison with FFT generated Reference Patterns

4.2 Average Power Pattern Matching per Number of Shots (SLL Variation Analysis)

To evaluate the QFFT precision in recreating power patterns, the pattern matching metric Γ_{avg} of Eq. 13 (and derived from the metric in Eq.9) is compared at parity of number of shots T for the three different SLL for the Dolph-Chebychev distribution.

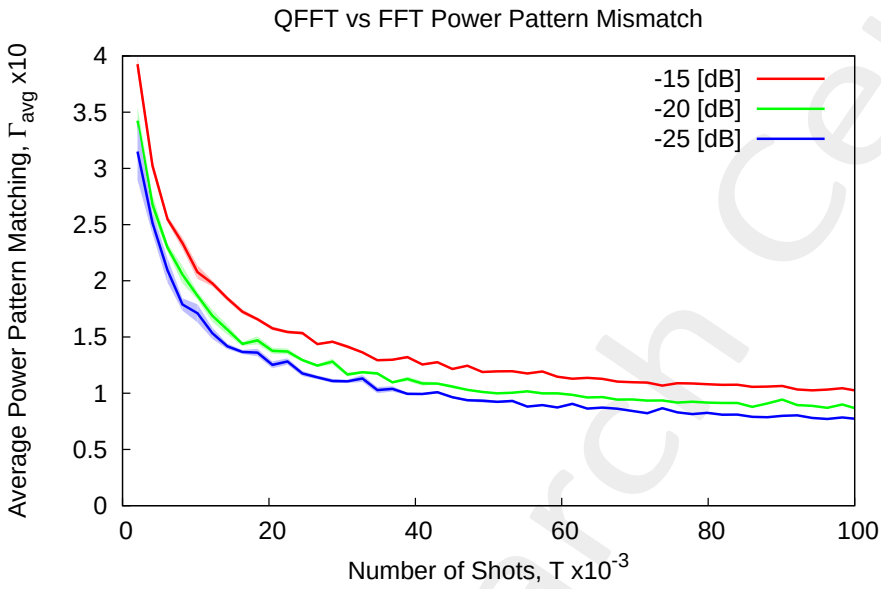

Figure 5: *Assessment - Shots variation analysis* ($N = 16$, $M = 1024$, Dolph-Chebychev pattern) - Average Power Pattern Mismatch Γ_{avg}comparison between patterns with $SLL = \{-15, -20, -25\}$ [dB] (*solid line*) $\pm$Variance (Γ_{var})$\times 10^2$ (*shaded region*)

Observations

From a theoretical point of view, the patterns with higher SLL should yield lower matching error, since (on the QFFT side) the resolution needed to represent higher probabilities is lower. In the analysis however, the opposite result is shown. The possible cause lays in the fact that the major contribution in the error is intrinsically given by the samples on the main lobe of the power patterns; however even at low values of T, the main lobe is fairly well approximated for all patterns, as the related QFFT samples have higher probability of being measures. This also implies that most of the Side Lobes region of the pattern is left entirely uncovered by the QFFT samples, meaning that the error (in the Side Lobes region of the pattern) could be approximated as the integral of the power over the Side Lobes. Finally, being the power over the Side Lobes lower for patterns lower SLL, the error will be smaller because the power over said regions is effectively lower rather than because it is better recreated by the QFFT.

4.2.1 Complexive Power Pattern Matching Metric Evaluation - Non Normalized Metric

In order to put in evidence the behaviour of the Power Pattern Matching metric, the a non normalized version of Γ, $\Gamma^{'}$ has been used:

$$\Gamma^{'} = \sum_{u=-1}^{u=1} \left| |E_{ref}(u)|^2 - P^{(T)}_{QFFT}(u) \right| \tag{17}$$

The result for the computation of $\Gamma'_{avg}$is reprted in the following figure:

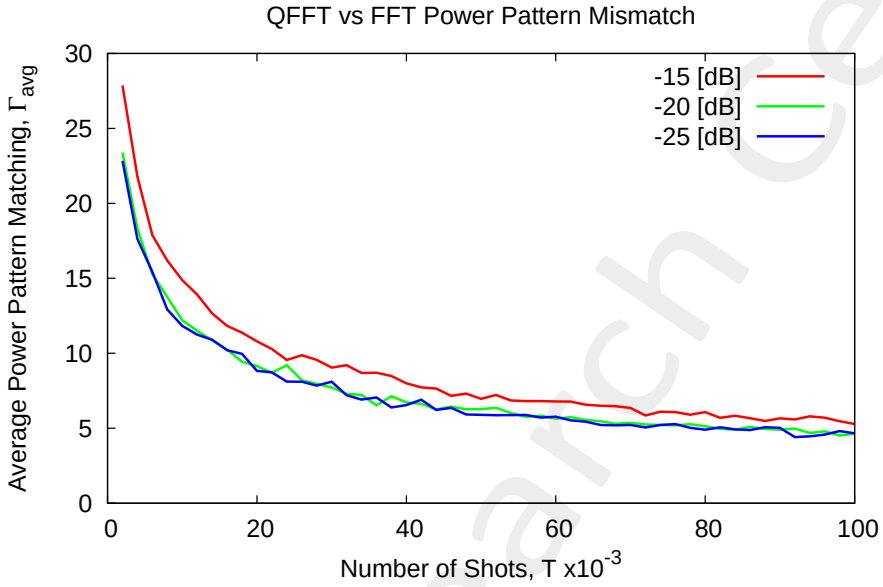

Figure 6: *Assessment - Shots variation analysis* ($N = 16$, $M = 1024$, $T \in \left[2.048 \times 10^3 : 1.024 \times 10^6\right]$) - Average Power Pattern Mismatch Γ'_{avg}comparison between patterns with $SLL = \{-15, -20, -25\}$ [dB]

The displacement of the curves, however is the same as the ones computed using Γ.

4.2.2 Partial Power Pattern Matching Metric Evaluation

Using the formulas of equations 10, 11 and 12, error is split into ML, and SL region and their sum, namely the total error.

Array Parameters:

- Number of elements (N): 16
- Elements spacing (d): $\lambda/2$
- Excitation Distribution: Dolph-Chebychev (Real Excitations)
- SLL cases: -15, -20, -25 [dB]

DFT/QFFT Parameters:

- Number of DFT points (M):1024
- Shots interval $[T_{min} : T_{max}]$: $T_{min} = 2.048 \times 10^3 (M \times 2)$, $T_{max} = 1.024 \times 10^6 (M \times 1000)$
- QFFT repetitions (R): 20

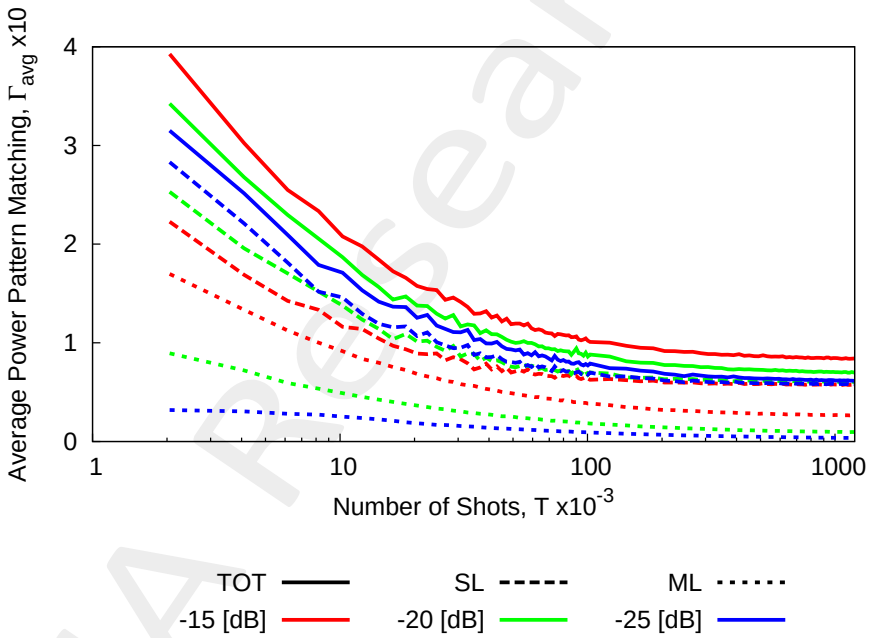

Figure 7: *Assessment - Shots variation analysis* ($N = 16$, $M = 1024$, $T \in [2.048 \times 10^3 : 1.024 \times 10^6]$) - Average Power Pattern Mismatch Γ_{avg} comparison between patterns with $SLL = \{-15, -20, -25\}$ [dB], divided into Γ_{TOT}, Γ_{SL} and Γ_{ML}

	$T = 2.048 \times 10^3$, $(M \times 2)$			$T = 8.192 \times 10^4$, $(M \times 80)$			$T = 1.204 \times$	
SLL	Γ_{SL}	Γ_{ML}	Γ_{TOT}	Γ_{SL}	Γ_{ML}	Γ_{TOT}	Γ_{SL}	Γ
-15	2.228×10^{-1}	1.698×10^{-1}	3.926×10^{-1}	6.697×10^{-2}	4.052×10^{-2}	1.075×10^{-1}	5.769×10^{-2}	2.682
-20	2.530×10^{-1}	8.942×10^{-1}	3.424×10^{-1}	7.107×10^{-2}	2.029×10^{-2}	9.136×10^{-2}	6.054×10^{-2}	9.765
-25	2.831×10^{-1}	3.186×10^{-2}	3.150×10^{-1}	7.078×10^{-2}	1.016×10^{-2}	8.094×10^{-2}	5.800×10^{-2}	3.746

Table I: *Assessment* - ($N = 16$, $M = 1024$, $T \in [2.048 \times 10^3 : 1.024 \times 10^6]$) - Average Power Pattern Mismatch Γ_{avg} comparison between patterns with $SLL = \{-15, -20, -25\}$ [dB], divided into Γ_{TOT}, Γ_{SL} and Γ_{ML} at T_{min}, T_{max} and $\hat{T}$

Observations

From the simulations of the figure few observations can be made:

1. Γ_{SL} is on average higher for lower SLL, proving the concept that higher T is required in order to obtain better representation of lower probability states.

2. Γ_{ML} is on average lower for lower SLL: this is due to the fact that in lower SLL patterns the size of the ML is greater with respect to higher ones. This observation can be formalized by stating that lowe SLL implies larger Half Power Beamwidth ($HPBW$), therefore implying that a greater number of high probability states is present in the main lobe of a low SLL pattern. From this last point, it is clear that to represent the ML of patterns with larger $HPBW$ fewer shots are necessary.

3. Γ_{TOT} is still greater for lower SLL, contrarily to what is expected, but this is justified as it is the sum of Γ_{SL} and Γ_{ML}.

4.3 Error Analysis for Pattern Representation Reliability

In order to show correlation between matching error and power patterns afforded by the QFFT, a pattern is taken as reference to define what a satisfactory representation looks like, toghether with $\Gamma_{avg}^{(T)}$ at the T used to compute it.

4.3.1 Total Error Γ_{TOT}

The reference pattern is the Dolph-Chebychev with $SLL = -15$ [dB] computed with $T_{ref} = 1.024 \times 10^6$ shots; the average error at T_{ref}, namely Γ_{ref} is 8.451×10^{-2}

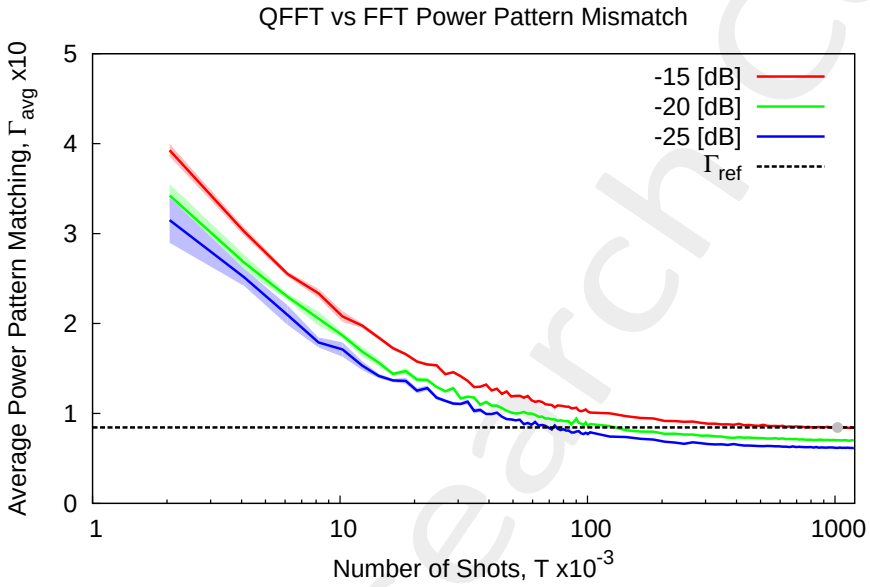

Figure 8: *Assessment - Shots variation analysis* ($N = 16$, $M = 1024$, $T \in \left[2.048 \times 10^3 : 1.024 \times 10^6\right]$) - Average Power Pattern Mismatch Γ_{avg}comparison between patterns with $SLL = \{-15, -20, -25\}$ [dB], compared to reference error Γ_{ref}

- The value of Γ_{ref} is first reached by the $SLL = -20$[dB] pattern at $\hat{T} = 1.4336 \times 10^5$ ($M \times 140$) shots, ($\Gamma_{avg} = 8.131 \times 10^{-2}$)
- The value of Γ_{ref} is first reached by the $SLL = -25$[dB] pattern at $\hat{T} = 6.9632 \times 10^4$ ($M \times 68$) shots, ($\Gamma_{avg} = 8.425 \times 10^{-2}$)

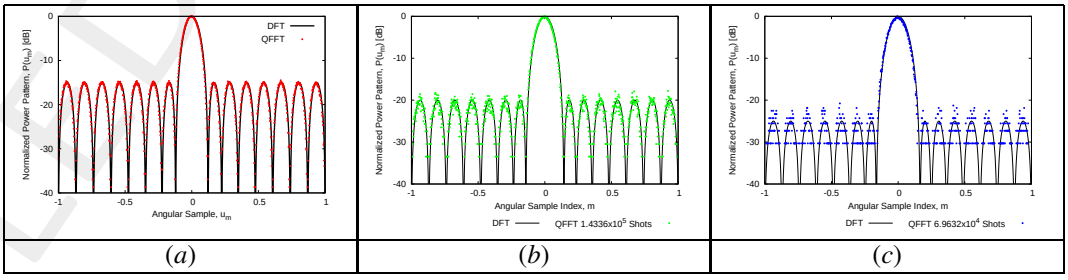

Figure 9: *Assessment - Shots variation analysis* ($N = 16$, $M = 1024$, $T \in \left[2.048 \times 10^3 : 1.024 \times 10^6\right]$) - QFFT computed power pattern at $\hat{T}$ shots when first reaching Γ_{ref} for $SLL = \{-15\,(a), -20\,(b), -25\,(c)\}$ [dB]

As can be noticed from the curves, lower SLL reach the target Γ_{ref} before the reference, however, pattern representation is not as precise as with $SLL = -15$ [dB]. In the following figures sample patterns at $T = 1.024 \times 10^6$ shots are reported:

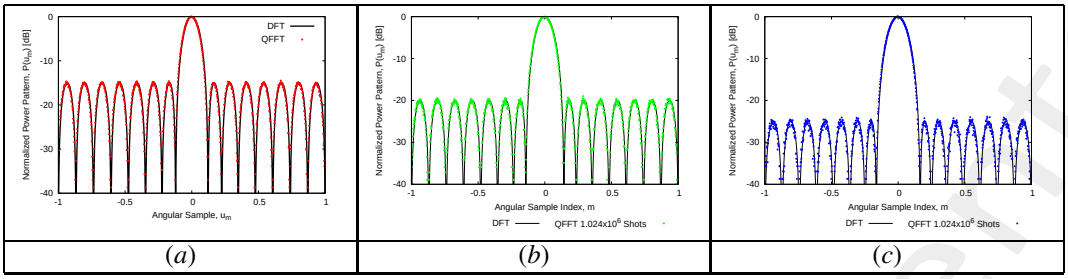

(*a*) (*b*) (*c*)

Figure 10: *Assessment - Shots variation analysis* ($N = 16$, $M = 1024$, $T \in \left[2.048 \times 10^3 : 1.024 \times 10^6\right]$) - QFFT computed power pattern with $T = 1.024 \times 10^6$ shots for $SLL = \{-15\ (a), -20\ (b), -25\ (c)\}$ [dB]

4.3.2 Side Lobes Error Γ_{SL}

The reference pattern is the Dolph-Chebychev with $SLL = -15$ [dB] computed with $T_{ref} = 1.024 \times 10^6$ shots; the average error at T_{ref}, namely Γ_{SL}^{ref} is 5.769×10^{-2}

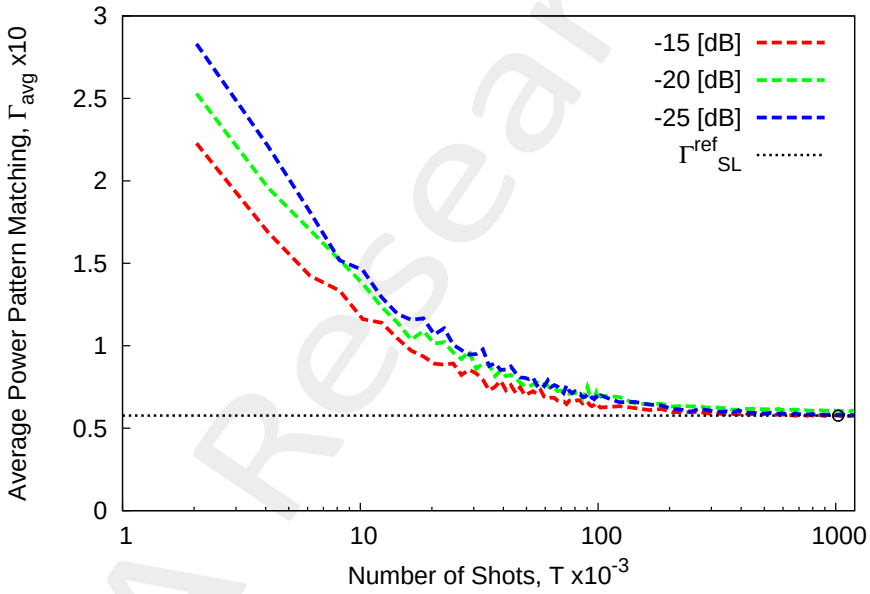

Figure 11: *Assessment - Shots variation analysis* ($N = 16$, $M = 1024$, $T \in \left[2.048 \times 10^3 : 1.024 \times 10^6\right]$) - Average Power Pattern Mismatch Γ_{SL}^{avg} comparison between patterns with $SLL = \{-15, -20, -25\}$ [dB], compared to reference error Γ_{SL}^{ref}

- The value of Γ_{ref} is not reached by the $SLL = -20$ [dB] pattern, however, at $\hat{T} = 1.024 \times 10^4$ ($M \times 10000$) shots, average SL error is $\Gamma_{SL}^{avg} = 5.991 \times 10^{-2}$
- The value of Γ_{ref} is first reached by the $SLL = -25$ [dB] pattern at $\hat{T} = 2.4576 \times 10^6$ ($M \times 2400$) shots, ($\Gamma_{SL}^{avg} = 5.769 \times 10^{-2}$)

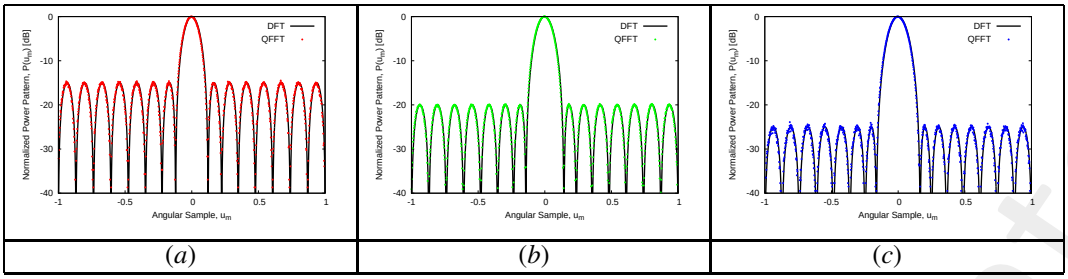

Figure 12: *Assessment - Shots variation analysis* ($N = 16$, $M = 1024$, $T \in \left[2.048 \times 10^3 : 1.024 \times 10^6\right]$) - QFFT computed power pattern at $\hat{T}$ shots when first reaching Γ_{ref} for $SLL = \{-15\,(a), -20\,(b), -25\,(c)\}$ [dB]

4.3.3 Main Lobe Error Γ_{ML}

The reference pattern is the Dolph-Chebychev with $SLL = -15$ [dB] computed with $T_{ref} = 1.024 \times 10^6$ shots; the average error at T_{ref}, namely Γ_{ML}^{ref} is 2.682×10^{-2}

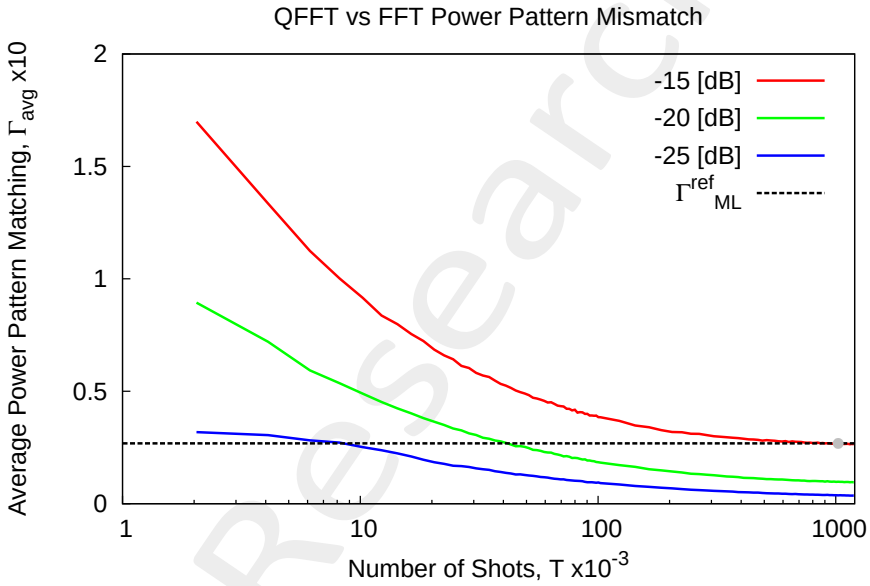

Figure 13: *Assessment - Shots variation analysis* ($N = 16$, $M = 1024$, $T \in \left[2.048 \times 10^3 : 1.024 \times 10^6\right]$) - Average Power Pattern Mismatch Γ_{ML}^{avg} comparison between patterns with $SLL = \{-15, -20, -25\}$ [dB], compared to reference error Γ_{ML}^{ref}

The value of Γ_{ref} is first reached by the $SLL = -20$ [dB] pattern at $\hat{T} = 4.3008 \times 10^4$ ($M \times 42$) shots, ($\Gamma_{ML}^{avg} = 2.635 \times 10^{-2}$)

- The value of Γ_{ref} is first reached by the $SLL = -25$ [dB] pattern at $\hat{T} = 1.024 \times 10^4$ ($M \times 10$) shots, ($\Gamma_{ML}^{avg} = 2.518 \times 10^{-2}$)

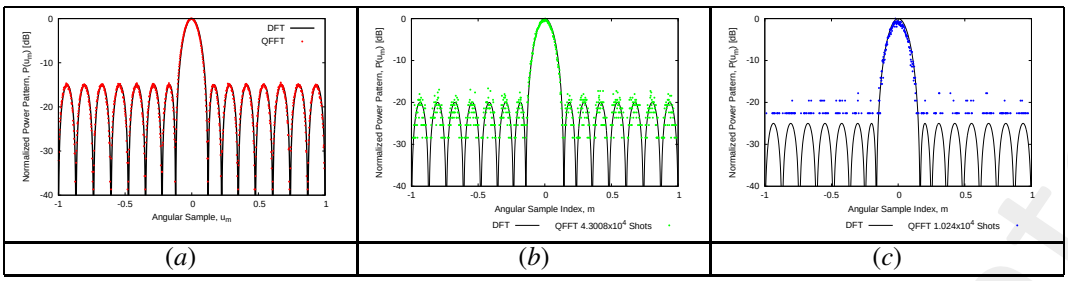

(*a*) (*b*) (*c*)

Figure 14: *Assessment - Shots variation analysis* ($N = 16$, $M = 1024$, $T \in \left[2.048 \times 10^3 : 1.024 \times 10^6\right]$) - QFFT computed power pattern at $\hat{T}$ shots when first reaching Γ_{ML}^{ref} for $SLL = \{-15\,(a), -20\,(b), -25\,(c)\}$ [dB]

4.4 Shaped Beams Assessment

QFFT based power pattern representation is carried out for shaped beams with both real and complex excitations. Validation is carried out also considering the impact of T on representation fidelity, by means of the partial error metric.

4.4.1 Taylor Pattern

Array Parameters:

- Number of elements (N): 16
- Elements spacing (d): $\lambda/2$
- Excitation Distribution: Taylor
- SLL -15 [dB],
- Controlled Lobes=4

DFT/QFFT Parameters:

- Number of DFT points (M):1024
- Shots interval $[T_{min} : T_{max}]$: $T_{min} = 2.048 \times 10^3 (M \times 2)$, $T_{max} = 1.024 \times 10^6 (M \times 10^3)$
- QFFT repetitions (R): 20

Shots Sensitivity Analysis

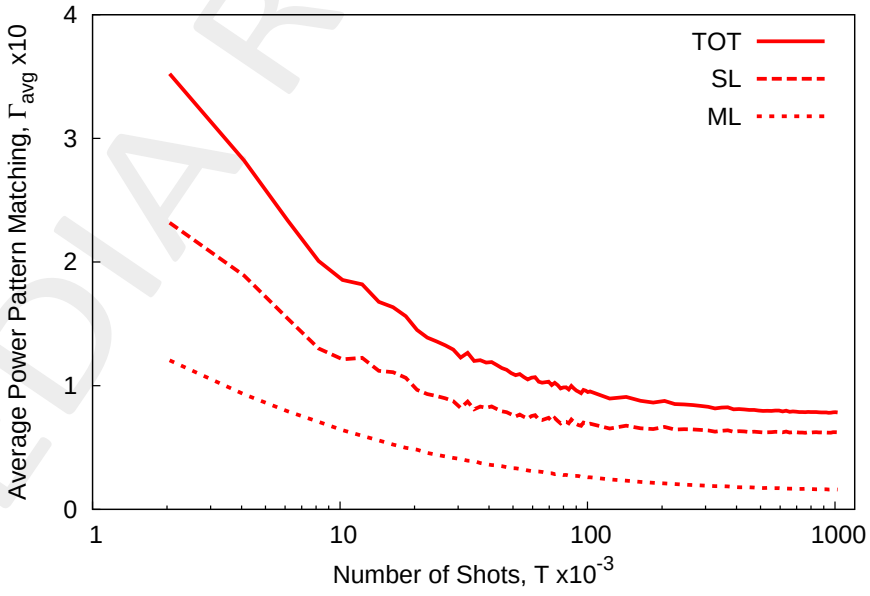

Figure 15: *Assessment* ($N = 16$, $M = 1024$, Taylor pattern) - Average Power Pattern Mismatch Γ_{avg} divided into Γ_{TOT}, Γ_{SL} and Γ_{ML}

T	Γ_{SL}	Γ_{ML}	Γ_{TOT}
$1.024 \times 10^4 (M \times 10)$	1.21×10^{-1}	6.409×10^{-2}	1.855×10^{-1}
$1.024 \times 10^5 (M \times 10^2)$	6.933×10^{-2}	2.602×10^{-2}	9.534×10^{-2}
$1.024 \times 10^4 (M \times 10^3)$	6.231×10^{-2}	1.609×10^{-2}	7.840×10^{-2}

Table II: *Assessment* ($N = 16$, $M = 1024$, Taylor pattern) - Relation between partial Γ_{avg} and T

Sample Power Patterns

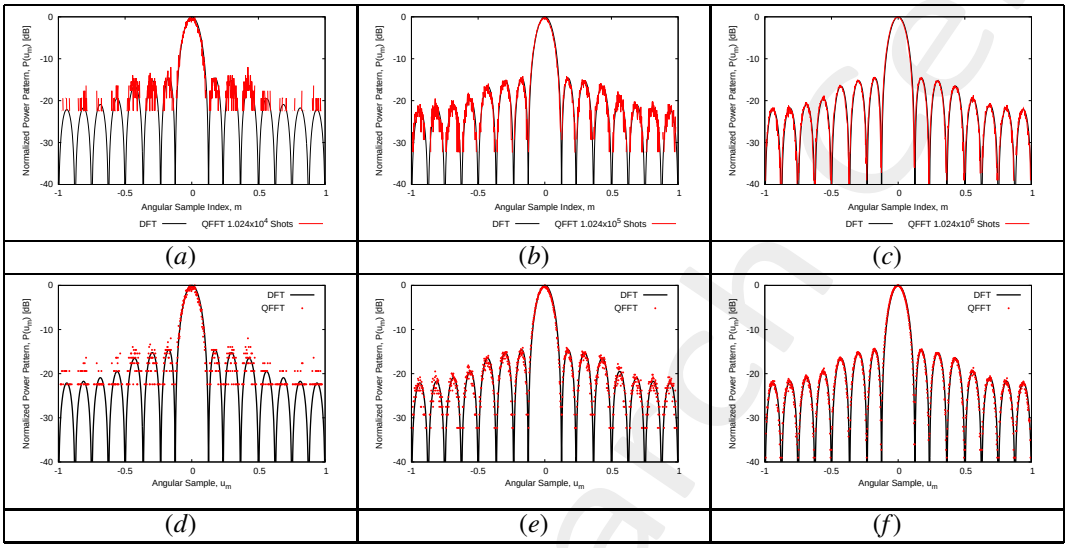

Figure 16: *Assessment - Pattern shape variation analysis* ($N = 16$, $M = 1024$, Taylor pattern) - Sample Power Pattern Representations at $T = 1.024 \times 10^4 (M \times 10)$ (*a*)(*d*), $T = 1.024 \times 10^5 (M \times 10^2)$ (*b*)(*e*), $T = 1.024 \times 10^6 (M \times 10^3)$ (*c*)(*f*)

4.4.2 Cosecant Squared Pattern

Array Parameters:

- Number of elements (N): 16
- Elements spacing (d): $\lambda/2$
- Excitation Distribution: Cosecant Squared
- SLL -20 [dB],

DFT/QFFT Parameters:

- Number of DFT points (M):1024
- Shots interval [T_{min} : T_{max}]: $T_{min} = 2.048 \times 10^3 (M \times 2)$, $T_{max} = 1.024 \times 10^6 (M \times 10^3)$
- QFFT repetitions (R): 20

Shots Sensitivity Analysis

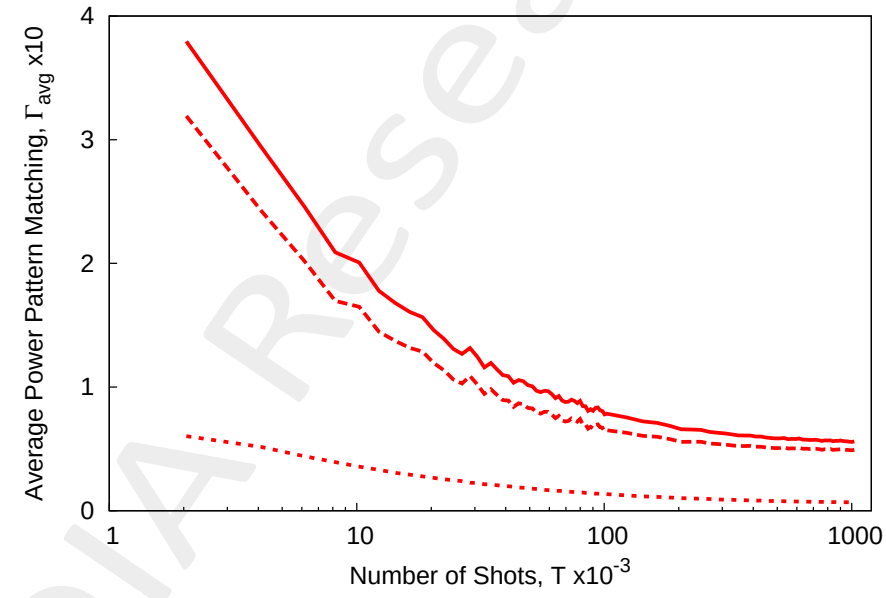

*

Figure 17: *Assessment - Pattern shape variation analysis* ($N = 16$, $M = 1024$, cosecant squared pattern) - Average Power Pattern Mismatch Γ_{avg} divided into Γ_{TOT}, Γ_{SL} and Γ_{ML}

T	Γ_{SL}	Γ_{ML}	Γ_{TOT}
$1.024 \times 10^4 (M \times 10)$	1.649×10^{-1}	3.571×10^{-2}	2.006×10^{-1}
$1.024 \times 10^5 (M \times 10^2)$	6.511×10^{-2}	1.342×10^{-2}	7.854×10^{-2}
$1.024 \times 10^4 (M \times 10^3)$	4.926×10^{-2}	6.763×10^{-2}	5.603×10^{-2}

Table III: *Assessment* ($N = 16$, $M = 1024$, cosecant squared pattern) - Relation between partial Γ_{avg} and T

Sample Power Patterns

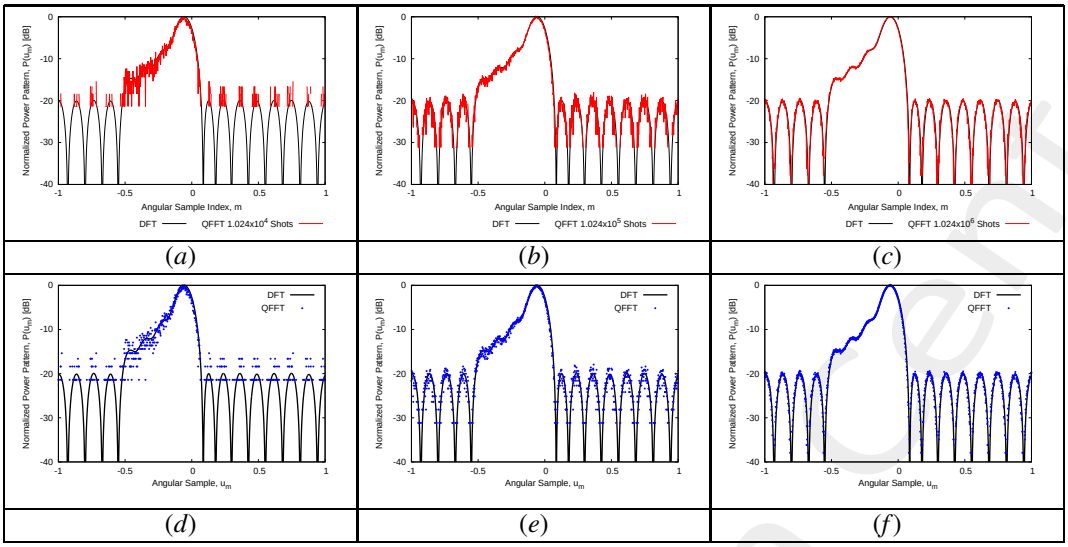

Figure 18: *Assessment - Pattern shape variation analysis* ($N = 16$, $M = 1024$, cosecant squared pattern) - Sample Power Pattern Representations at $T = 1.024 \times 10^4 (M \times 10)$ $(a)(d)$, $T = 1.024 \times 10^5 (M \times 10^2)$ $(b)(e)$, $T = 1.024 \times 10^6 (M \times 10^3)$ $(c)(f)$

4.4.3 Flat Top Beam Pattern

Array Parameters:

- Number of elements (N): 16
- Elements spacing (d): $\lambda/2$
- Excitation Distribution: Flat Top Main Beam
- SLL -20 [dB],

DFT/QFFT Parameters:

- Number of DFT points (M):1024
- Shots interval [$T_{min} : T_{max}$]: $T_{min} = 2.048 \times 10^3 (M \times 2)$, $T_{max} = 1.024 \times 10^6 (M \times 10^3)$
- QFFT repetitions (R): 20

Shots Sensitivity Analysis

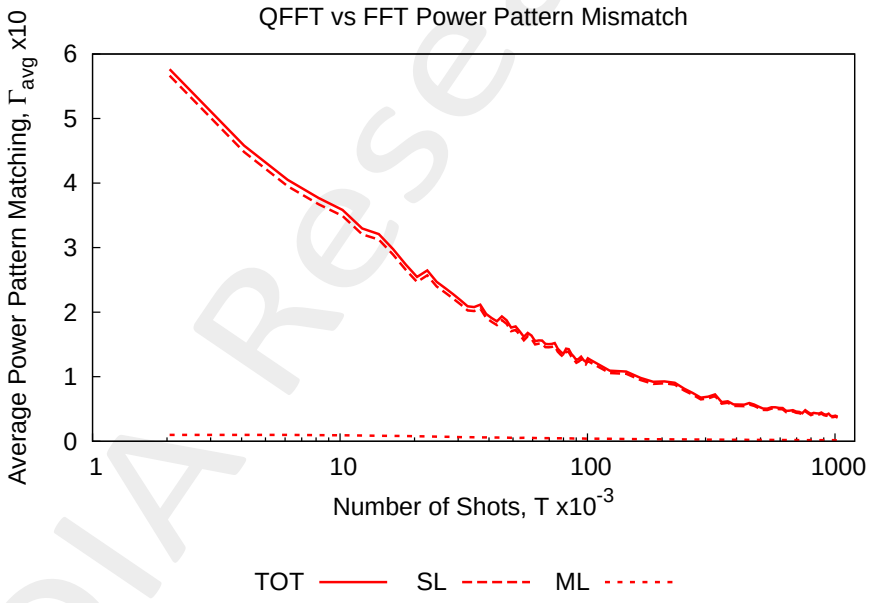

Figure 19: *Assessment* ($N = 16$, $M = 1024$, flat top beam pattern) - Average Power Pattern Mismatch Γ_{avg} divided into Γ_{TOT}, Γ_{SL} and Γ_{ML}

T	Γ_{SL}	Γ_{ML}	Γ_{TOT}
$1.024 \times 10^4 (M \times 10)$	3.491×10^{-1}	9.218×10^{-3}	3.583×10^{-1}
$1.024 \times 10^5 (M \times 10^2)$	1.225×10^{-1}	4.016×10^{-3}	1.265×10^{-1}
$1.024 \times 10^4 (M \times 10^3)$	3.656×10^{-2}	1.629×10^{-3}	3.818×10^{-2}

Table IV: *Assessment* ($N = 16$, $M = 1024$, flat top beam pattern) - Relation between partial Γ_{avg} and T

Sample Power Patterns

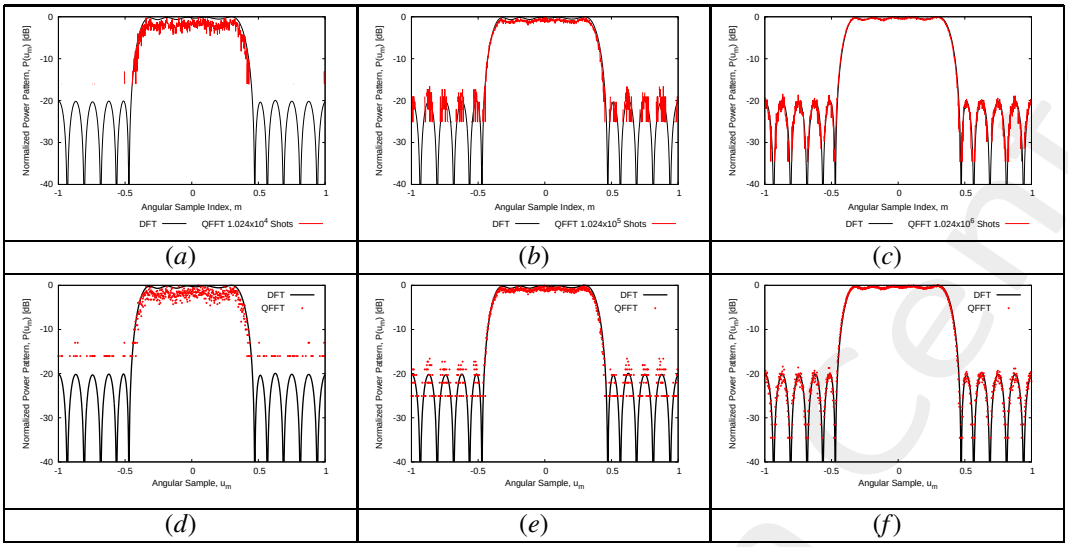

Figure 20: *Assessment - Pattern shape variation analysis* ($N = 16$, $M = 1024$, flat top beam pattern) - Sample Power Pattern Representations at $T = 1.024 \times 10^4 (M \times 10)$ $(a)(d)$, $T = 1.024 \times 10^5 (M \times 10^2)$ $(b)(e)$, $T = 1.024 \times 10^6 (M \times 10^3)$ $(c)(f)$

5 Real Quantum Computer Assessment

In this section the previously simulated derivation of the Power Pattern by means of the QFFT is tested on real quantum computers provided by IBM.

Each quantum computer is characterized by its number of qubits, and useful informations provided by IBM are its average error on CNOT ports (CE) together with the time elapsed from the last recalibration (TER).

As in real quantum computers noise has a strong influence, ad hoc test cases are designed in order to show the actual correlation between inputs and outputs of the QC programs.

M=32, N=4, Uniform Excitations

One of the sets of QC available at IBM have $L = 5$ qubits, therefore a first test is carried out on small scale arrays with few DFT points.

In the following figure are reported the visual representations of the results, with the specification of the QC used with its approximate recalibration time when the program has been executed and the average error probability on the single CNOT gate[(1)]:

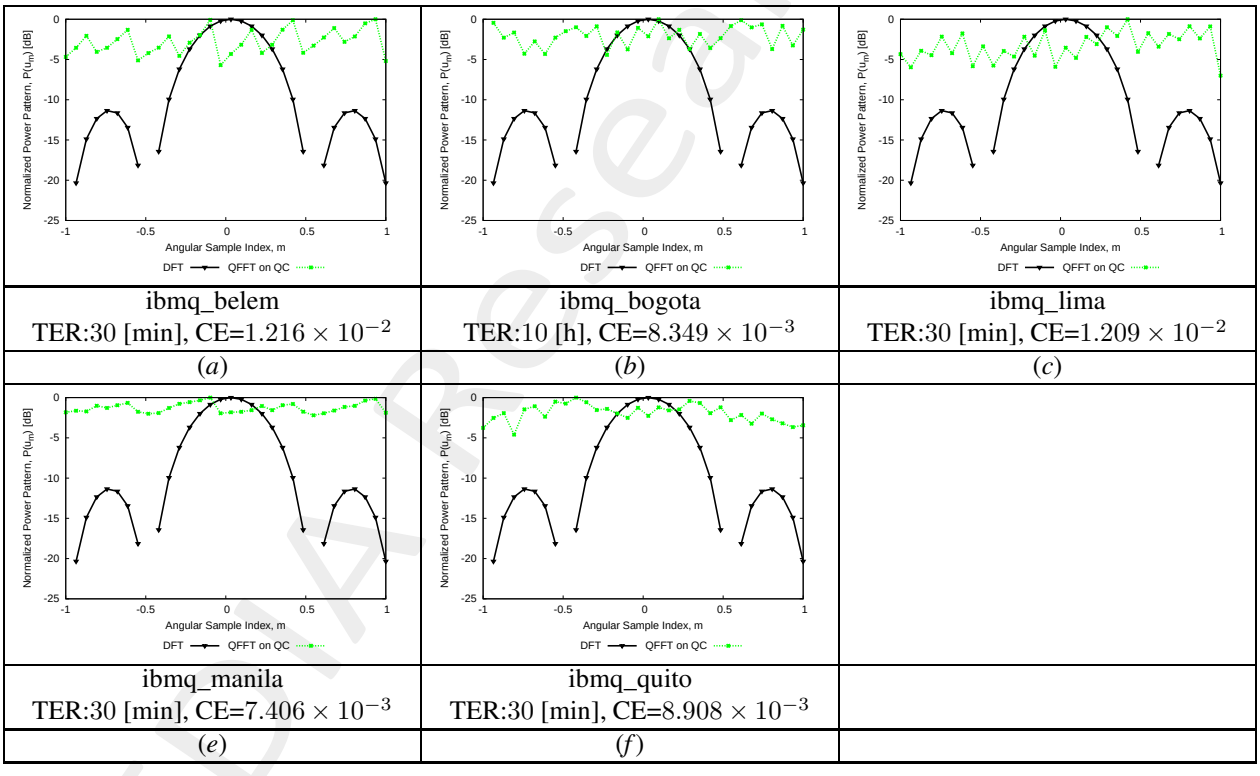

ibmq_belem TER:30 [min], CE=1.216×10^{-2}	ibmq_bogota TER:10 [h], CE=8.349×10^{-3}	ibmq_lima TER:30 [min], CE=1.209×10^{-2}
(*a*)	(*b*)	(*c*)
ibmq_manila TER:30 [min], CE=7.406×10^{-3}	ibmq_quito TER:30 [min], CE=8.908×10^{-3}	
(*e*)	(*f*)	

Figure 21: *Real QC Assessment* ($N = 4$, $M = 32$, uniform excitations) - Real QC results

[(1)]Note: The error is provided for a single gate, while in transpiled circuits many gates are put in cascade, making the error probability grow very quickly.

6 Complexity Evaluation

Let us consider the classical procedure for the computation of the PA power pattern, consisting in applying the DFT on a set of M values and consequently the modulus squared. The complexity can thereby be analyzed as the sum of the complexity of the DFT, the modulus and the power 2 elevation, with complexities:

- DFT (FFT implementation): $O(Mlog(M))$
- Modulus (supposing fixed time execution, i.e, application of the operation takes the same time for each instance): $O(M)$
- Power 2 elevation (supposing fixed time execution): $O(M)$

The total complexity becomes $C_{classical} = O(Mlog(M)) + O(M) + O(M) = O(Mlog(M)) + O(2M)$ which, up to constant factors, becomes:

$$C_{classical} = O(M(log(M) + 1)) \tag{18}$$

In the QFFT case the operation only consists in applying the QFFT, therefore, the total complexity is the one of the QFFT algoritm, namely:

$$C_{quantum} = C_{QFFT} = O(log(M)^2) \tag{19}$$

The complexity ratio can therefore be computed as:

$$\frac{C_{classical}}{C_{quantum}} = \frac{M(log(M) + 1)}{log(M)^2} \tag{20}$$

7 Conclusions

In order to be able to correctly assess the precision of the QFFT algorithm in replicating the DFT results a new power pattern matching metric should be implemented, in order to:

1. Take appropriately into account the regions in which no QFFT sample is present (i.e. states for which $\mu_m = p_m = 0$) for the computation of the metric
2. Give appropriate weight to error due to samples in the side lobe regions

A method to define the sufficient precision of the QFFT power pattern computation should be devised, since simple the Γ_{avg} based threshold is not representative of the actual computation fidelity.

More information on the topics of this document can be found in the following list of references.

References

[1] L. Tosi and P. Rocca, “Antenna array analysis through universal quantum computing processors - A study on noise modeling and impact," *IEEE Transactions on Microwave Theory and Techniques*, vol. 72, no. 4, pp. 2067-2083, April 2024 (DOI:10.1109/TMTT.2023.3344878).

[2] L. Tosi, P. Rocca, N. Anselmi, and A. Massa, “Array antenna power pattern analysis through quantum computing,” *IEEE Trans. Antennas Propag.* , vol. 71, no. 4, pp. 3251-3259, Apr. 2023.

[3] P. Rocca, N. Anselmi, G. Oliveri, A. Polo, and A. Massa, “Antenna array thinning through quantum Fourier transform," *IEEE Access*, vol. 9, pp. 124313-124323, 2021.

[4] P. Rocca, N. Anselmi, A. Polo, and A. Massa, “Pareto-optimal domino-tiling of orthogonal polygon phased arrays,” *IEEE Trans. Antennas Propag.*, vol. 70, no. 5, pp. 3329-3342, May 2022.

[5] P. Rocca, N. Anselmi, A. Polo, and A. Massa, “An irregular two-sizes square tiling method for the design of isophoric phased arrays," *IEEE Trans. Antennas Propag.*, vol. 68, no. 6, pp. 4437-4449, Jun. 2020.

[6] N. Anselmi, L. Tosi, P. Rocca, G. Toso, and A. Massa, “A self-replicating single-shape tiling technique for the design of highly modular planar phased arrays - The case of L-shaped rep-tiles,” *IEEE Trans. Antennas Propag.* , vol. 71, no. 4, pp. 3335-3348, Apr. 2023.

[7] A. Benoni, P. Rocca, N. Anselmi, and A. Massa, “Hilbert-ordering based clustering of complex-excitations linear arrays," *IEEE Trans. Antennas Propag.* , vol. 70, no. 8, pp. 6751-6762, Aug. 2022.

[8] P. Rocca, L. Poli, N. Anselmi, and A. Massa, “Nested optimization for the synthesis of asymmetric shaped beam patterns in sub-arrayed linear antenna arrays," *IEEE Trans. Antennas Propag.* , vol. 70, no. 5, pp. 3385 - 3397, May 2022.

[9] P. Rocca, L. Poli, A. Polo, and A. Massa, “Optimal excitation matching strategy for sub-arrayed phased linear arrays generating arbitrary shaped beams," *IEEE Trans. Antennas Propag.*, vol. 68, no. 6, pp. 4638-4647, Jun. 2020.

[10] M. Salucci, G. Oliveri, and A. Massa, “An innovative inverse source approach for the feasibility-driven design of reflectarrays," *IEEE Trans. Antennas Propag.* , vol. 70, no. 7, pp. 5468-5480, July 2022.

[11] G. Ding, N. Anselmi, W. Xu, P. Li, and P. Rocca, “Interval-bounded optimal power pattern synthesis of array antenna excitations robust to mutual coupling," *IEEE Antennas Wireless Propag. Lett.*, IEEE Antennas Wireless Propag. Lett., vol. 22, no. 11, pp. 2725-2729, Nov. 2023.

[12] N. Anselmi, P. Rocca, and A. Massa, “Tolerance analysis of reconfigurable monopulse linear antenna arrays through interval arithmetic," *J. Electromagn. Waves Appl. J*, pp. 1066-1081, 2023.

[13] P. Rocca, N. Anselmi, A. Benoni, and A. Massa, “Probabilistic interval analysis for the analytic prediction of the pattern tolerance distribution in linear phased arrays with random excitation errors," *IEEE Trans. Antennas Propag.*, vol. 68, no. 2, pp. 7866-7878, Dec. 2020.

[14] P. Rocca, N. Anselmi, M. A. Hannan, and A. Massa, “Conical frustum multi-beam phased arrays for air traffic control radars," *Sensors*, vol. 22, no. 19, 7309, pp. 1-18, 2022.

[15] F. Zardi, G. Oliveri, M. Salucci, and A. Massa, “Minimum-complexity failure correction in linear arrays via compressive processing," *IEEE Trans. Antennas Propag.*, vol. 69, no. 8, pp. 4504-4516, Aug. 2021.

[16] P. Rocca, N. Anselmi, A. Polo, and A. Massa, “Modular design of hexagonal phased arrays through diamond tiles,” *IEEE Trans. Antennas Propag*., vol.68, no. 5, pp. 3598-3612, May 2020.

[17] N. Anselmi, L. Poli, P. Rocca, and A. Massa, “Design of simplified array layouts for preliminary experimental testing and validation of large AESAs," *IEEE Trans. Antennas Propag.*, vol. 66, no. 12, pp. 6906-6920, Dec. 2018.

[18] N. Anselmi, P. Rocca, M. Salucci, and A. Massa, “Contiguous phase-clustering in multibeam-on-receive scanning arrays," *IEEE Trans. Antennas Propag.*, vol. 66, no. 11, pp. 5879-5891, Nov. 2018.

[19] G. Oliveri, G. Gottardi and A. Massa, “A new meta-paradigm for the synthesis of antenna arrays for future wireless communications," *IEEE Trans. Antennas Propag.*, vol. 67, no. 6, pp. 3774-3788, Jun. 2019.

[20] P. Rocca, M. H. Hannan, L. Poli, N. Anselmi, and A. Massa, “Optimal phase-matching strategy for beam scanning of sub-arrayed phased arrays," *IEEE Trans. Antennas and Propag.*, vol. 67, no. 2, pp. 951-959, Feb. 2019.

[21] M. Salucci, G. Gottardi, N. Anselmi, and G. Oliveri, “Planar thinned array design by hybrid analytical-stochastic optimization," *IET Microwaves, Antennas & Propagation*, vol. 11, no. 13, pp. 1841-1845, Oct. 2017

[22] P. Rocca, G. Oliveri, R. J. Mailloux, and A. Massa, “Unconventional phased array architectures and design Methodologies - A review," *Proc. IEEE*, vol. 104, no. 3, pp. 544-560, March 2016.